

# Atomistic Simulation of Orientation-dependent Tension Deformation Behavior of Single Crystal Iridium

Yang Jieren<sup>1</sup>, Wang Hu<sup>1</sup>, Hu Rui<sup>1</sup>, Zhang Fan<sup>3</sup>, Li Shuangming<sup>1</sup>, Liu Yi<sup>2</sup>, Luo Ximing<sup>2</sup>

<sup>1</sup> State Key Laboratory of Solidification Processing, Northwestern Polytechnical University, Xi'an 710072, China; <sup>2</sup> Kunming Institute of Precious Metals, Kunming 650106, China; <sup>3</sup> Baoji University of Art and Sciences, Baoji 721016, China

**Abstract:** Single crystal iridium exhibits anomalous deformation behaviors in contrast to other fcc-metals and its intrinsic deformation mechanism is still controversial. To investigate the deformation behaviors and underlying deformation mechanisms with respect to crystallographic orientations in single crystal iridium, the molecular dynamics simulations were performed at 1 K to simulate the tensile deformation behavior of bulk single crystal iridium in different loading axis orientations of [100], [110] and [111]. Atomic simulation results show that the stress-strain curves differ significantly in three crystallographic orientations. And the mechanical properties including elastic modulus, yield stress, ultimate tensile stress and elongation are more or less different in different crystallographic orientations owing to different deformation mechanisms. Under tensile loading, [100] oriented single crystal iridium deforms predominantly by dislocation slide and partial vacancy coalescence, while plastic deformation in [110] oriented single crystal iridium is initiated by stacking faults. Nevertheless, [111] oriented single crystal iridium undergoes little plastic deformation before breaking.

**Key words:** single crystal iridium; molecular dynamics; tensile deformation; crystallographic orientation

Due to the exceptional high-temperature strength and high resistance to corrosion at elevated temperatures [1-3], iridium has drawn considerable attention to ultra-high temperature structural applications [4] in aggressive media during the past few decades. Unfortunately, unlike the good ductility of other fcc-metals, iridium exhibits poor workability. Under tensile loading, single crystal iridium undergoes brittle transgranular cleavage after considerable plastic strain at room temperature [5, 6], while polycrystalline iridium fails predominantly through intergranular fracture at temperatures up to 1000 °C [7, 8]. Although plenty of efforts have been made to explore the deformation and brittle fracture mechanism of single crystal iridium, it is still controversial in the materials science community, so further elucidating its intrinsic mechanism is scientifically important and technologically valuable.

Previous experimental studies show that single crystal

iridium exhibits apparent plastic anisotropy when subjected to tensile deformation [9, 10]. The elongation along [110] orientation is 30%~40%, which is only 10%~12% along [100] orientation [9]. However, those experiments cannot determine what processes occur on the atomistic scale in real time. Besides, above experimental researches are usually restricted to the experimental means since the capture of the investigation of deformation mechanisms by performing experiments at nanoscale is always difficult and challenging.

With the advances in computational capability and the availability of reliable inter-atomic potentials [11], molecular dynamics (MD) simulation is an alternative approach to evaluate such atomic-scale processes and provide the atomistic level details of deformation and fracture mechanism in multiple materials during tensile deformation. Most of works involve strain rate [12-14], size [15-17], temperature [18-20]

Received date: May 09, 2018

Foundation item: National Key Research and Development Program of China (2017YFB0305503); National Natural Science Foundation of China (U1202273)  
Corresponding author: Hu Rui, Ph. D., Professor, State Key Laboratory of Solidification Processing, Northwestern Polytechnical University, Xi'an 710072, China, P. R. China, Tel: 0086-29-88492172, E-mail: rhu@nwpu.edu.cn

Copyright © 2019, Northwest Institute for Nonferrous Metal Research. Published by Science Press. All rights reserved.

and orientation effects [21-25]. In this respect, there are only a few studies regarding iridium [26,27], where atomistic simulations are employed to calculate the physical properties of iridium under pressure and temperature [26] and to investigate the dislocation core structure in iridium [27]. Hence, there is a lack of systematic and thorough study of deformation behaviors of iridium with respect to crystallographic orientations in the literature using this atomistic method so far.

The current study, by the mean of MD simulation, is to investigate the orientation dependences of deformation behavior of single crystal iridium, and to get a further understanding of the underlying deformation mechanism from an atomistic view.

## 1 Modelling and Methodology

### 1.1 Simulation models

In order to determine the orientation dependence of mechanical response and deformation mechanism in single crystal iridium, different tensile axial orientations of [100], [110] and [111] were considered. Fig.1 shows the tensile model created from a regular lattice of bulk fcc single crystal iridium along three different crystallographic orientations. Fig.1a shows the tension model along the [100] orientation which coincides with the  $x$ -axis, while  $y$  and  $z$  axes are taken as [010] and [001] crystallographic orientations, respectively. The dimension is  $20a_0 \times 15a_0 \times 15a_0$  corresponding to 18 000 atoms, where  $a_0=0.384$  nm is the lattice constant of iridium. For the second [110] tension model, as shown in Fig.1b, the axes ( $x, y, z$ ) coincide with crystallographic orientations according to  $x=[001]$ ,  $y=[\bar{1}10]$  and  $z=[110]$ , and the dimension is  $14 a_0 \times 10 \sqrt{2} a_0 \times 18 \sqrt{2} a_0$  containing 20 160 atoms. For the third [111] tension model, as shown in Fig.1c,  $x, y$  and  $z$  axes are taken as  $[1\bar{1}0]$ ,  $[11\bar{2}]$ ,  $[111]$  crystallographic orientations, respectively, and the dimension is  $8\sqrt{2} a_0 \times 4\sqrt{6} a_0 \times 20\sqrt{3} a_0$  containing 15 360 atoms.

### 1.2 Potential function

For fcc iridium, the interaction among the constituent atoms was described using the embedded atom method (EAM) potential proposed by Sheng and co-workers [28]. The potential was developed by fitting the potential-energy surface of iridium (involving lattice dynamics, mechanical properties, thermal behavior, energetics of competing crystal structures, defects, deformation paths, liquid structures) via high-precision first-principle calculations, which is suitable for high-quality atomistic computer simulation of practical applications owing to high fidelity and robustness.

In the EAM potential, essentially, an atom is regarded to be embedded into the background electrons provided by all other neighboring atoms in the system. The EAM potential can be given by:

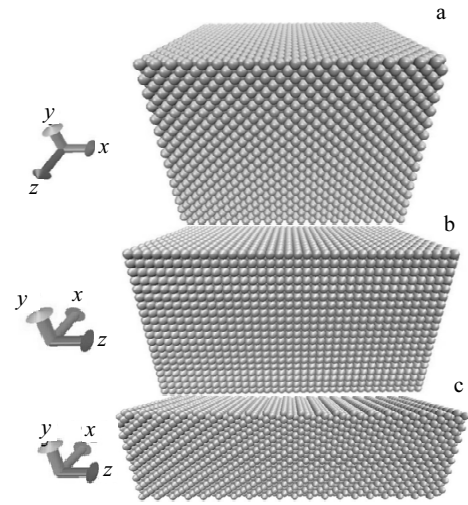


Fig.1 Tensile models of single crystal iridium with [100] orientation (a), [110] orientation (b), and [111] orientation (c)

$$U_{\text{total}} = \sum_i U_i = \sum_i \left[ \frac{1}{2} \sum_{j \neq i} V(r_{ij}) + F(\rho_i) \right] \quad (1)$$

$$\rho_i = \sum_{j \neq i} \Phi_j(r_{ij}) \quad (2)$$

where  $U_{\text{total}}$  is the total potential energy of the system,  $U_i$  is the potential energy of atom  $i$ ,  $\rho_i$  is the host electron density around an isolated atom  $i$ ,  $V(r_{ij})$  is the pair repulsion between atoms  $i$  and  $j$ , which are separated by the distance of  $r_{ij}$ ,  $F(\rho_i)$  is the energy to embed atom  $i$  at an electron density  $\rho_i$ , and  $\Phi_j(r_{ij})$  is the electron density at atom  $i$  since atom  $j$  is as a function of the distance  $r_{ij}$ .

### 1.3 Stress calculations

The volume-averaged stresses  $\sigma_{\alpha\beta}$  in the atomic systems were calculated using the virial theorem [29] as follows:

$$\sigma_{\alpha\beta} = \frac{1}{\Omega} \left[ - \sum_i m_i v_i^\alpha v_i^\beta + \frac{1}{2} \sum_i \sum_{j \neq i} F_{ij}^\alpha F_{ij}^\beta \right] \quad (3)$$

where  $\alpha, \beta$  denote the three axes of Cartesian coordinate system,  $\alpha, \beta = x, y, z$ ,  $\Omega$  is the volume of the atomic system,  $m_i$  is the mass of atom  $i$ ,  $v_i^\alpha$  and  $v_i^\beta$  are the thermal excitation velocities of atom  $i$  in the  $\alpha$  and  $\beta$  directions, respectively.  $F_{ij}^\alpha$  and  $F_{ij}^\beta$  are the forces in the  $\alpha$  and  $\beta$  directions between atoms  $i$  and  $j$ , respectively. Therefore, the first and second terms on the right side of the above equation imply the thermal effect and atomistic interactions, respectively.

### 1.4 Simulation methods

MD simulations were performed in large-scale atomic/molecular massively parallel simulator (namely, LAMMPS) package [30] based on the classical statistical mechanics [31], while the visualization of the evolution of the atomic structures during tensile deformation was realized by OVITO software [32]. Detailed simulations of three

typical tensile directions oriented in [100], [110] and [111] were carried out, because these three selected cases can represent most of the typical stress-strain responses and deformation mechanisms of bulk single crystal iridium with different orientations.

In the simulations, an NVT-ensemble (systems with fixed pressure  $P$ , temperature  $T$ , and number of atoms  $N$ ) was used. To avoid thermal activation, all the MD simulations were performed at 1 K. Thermal velocities of the atoms were initialized using a Boltzmann distribution. Prior to loading, systems were gradually relaxed 80 000 steps to reach an equilibrium minimum energy configuration at 1 K. Periodic boundaries were applied along the  $x$ ,  $y$ ,  $z$  axes to eliminate the surface effects and to gain a realistic description of the deformation behavior of the nanostructures in the bulk single crystal iridium. After enough relaxation, the models were stretched at the strain rate of  $0.01 \text{ ps}^{-1}$  along a particular loading axis orientation ([100], [110] or [111] direction) at 1 K until the final rupture and corresponding mechanical quantities were recorded and solved. Systems were maintained at a constant temperature, which was achieved by scaling the instantaneous velocities of all atoms throughout the stretching process. The Newtonian motion equations were integrated by the Verlet-velocity algorithm<sup>[33]</sup> to obtain the velocity and trajectories of atoms, with a time step of  $1.0 \text{ fs}$  ( $10^{-15} \text{ s}$ ).

## 2 Results and Discussion

### 2.1 Mechanical responses under tension at 1 K

Fig.2 depicts the axial tensile stress-strain curves of [100], [110], and [111] oriented single crystal iridium. The deformation behavior differs remarkably between the loading axis orientations. The stress-strain curves of [110] and [111] single crystal iridium exhibit a similar tendency in the stretching process. Initially, the stresses increase linearly in the elastic stage. Then, a yielding deformation occurs corresponding to the incipiently irreversible deformation. The stresses increase gradually to the first peak value, and then abruptly decline to the vicinity of 15 GPa in the subsequent uniform plastic deformation stage. Subsequently, the single crystal iridium undergoes a strain hardening stage, in which the stresses increase gradually to the second peak. Finally, the stresses dramatically decline to zero, implying that some local fractures occur in the [100] and [110] oriented single crystals. In contrast to the [100] orientation, [110] orientation shows higher ultimate tensile stress and larger fracture strain. Different from the cases in [100] and [110] orientations, the tensile stress of [111] orientation increases linearly in the initial elastic region. Beyond the limitation, an irreversible deformation appears in the single crystal iridium. The stress increases continuously until its peak value is reached, and then a substantial drop with little fluctuation occurs. In summary, the deformation behaviors

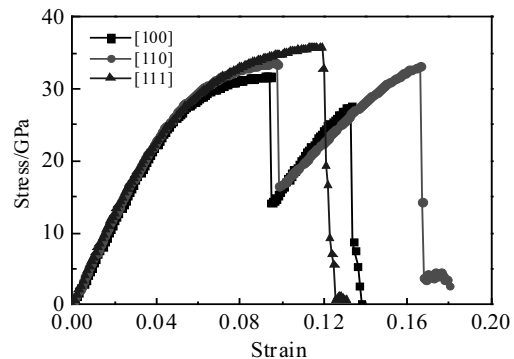


Fig.2 Stress-strain response of fcc single crystal iridium with different orientations under tension at 1 K

of single crystal iridium are strongly dependent on crystallographic orientations.

The yield stress point, in this study, was determined as the point at a strain level of 0.04 on the stress-strain curves, corresponding to the incipience of permanent deformation. While the ultimate tensile stress was defined as the first peak stress value, and the strain at which the second stress peak appears was considered as elongation of single crystal iridium.

The elastic properties of single crystal iridium at 1 K were evaluated, and its Young's modulus derived by fitting the data in the elastic region is 566.71, 574.57 and 569.63 GPa in [100], [110] and [111] orientations, respectively. The differences in Young's modulus with respect to orientation verify the elastic anisotropy in fcc single crystal iridium. The orientation dependence of Young's modulus results from the discrepancy of inter-atomic forces in three orientations<sup>[11]</sup>. The Young's modulus follows the order of  $E_{[110]} > E_{[111]} > E_{[100]}$ , demonstrating that atoms in [110] direction possess the strongest cohesive force in single crystal iridium, while the weakest in [100] direction.

Moreover, other mechanical properties, more or less, differ between loading axis orientations: single crystal iridium with [110] orientation shows the highest yield stress of 22.83 GPa followed by 22.65 GPa for the [111] orientation, while the [100] orientation shows the lowest yield stress of 22.37 GPa. In terms of ultimate tensile stress, it is 35.83 GPa for the [111] orientation and 33.64 GPa for the [110] orientation, but only 31.72 GPa for the [100] orientation, increasing in the order of [100], [110] and [111] orientations. Elongations of [100], [110] and [111] oriented single crystal iridium are 13.3%, 16.6% and 11.9%, respectively, following the order of  $\delta_{[110]} > \delta_{[111]} > \delta_{[100]}$ , demonstrating that according to the experimental study<sup>[9]</sup>, qualitatively, [110] orientation exhibits better ductility than [100] orientation.

## 2.2 Deformation mechanisms under tension at 1 K

Detailed differences in the curves imply that the orientation-dependence differs significantly for processes controlled by different mechanisms. To better understand the different deformation behaviors and reveal the intrinsic mechanisms behind these phenomena, the corresponding atomic arrangements at different deformation stages in various loading axis orientations are shown in Fig.3~6. In order to visualize interior defects, the surface atoms were removed from the perfect fcc structures.

### 2.2.1 [100] orientation

The atomic configurations of [100] oriented single crystal iridium at various strain levels during tensile deformation are presented in Fig.3. Single crystal iridium yields at a strain level of 0.093 (see Fig.2), where iridium atoms deviate from the equilibrium position for small displacements, displaying a relatively organized atomic arrangement as shown in Fig.3a. When the strain value increases to 0.095, as shown in Fig.3b, surface steps caused by dislocation slide appear at the top and bottom surfaces of fcc iridium crystal. As shown in Fig.3c, the cutaway view of atomic configurations on (010) plane in the [100] oriented tensile model involves many dislocation slips as well as partial vacancy coalescence, which consumes partial systematic energy and results in a sharp drop in stress from the first peak value to a low stress value (see Fig.2). Once the strain exceeds 0.133, local necking appears, and the model eventually breaks at the strain of 0.138, causing a drastic drop in stress. Fig.3d illustrates details of atomic arrangement at fi-

nal rupture. Flat triangular fracture can be clearly observed, manifesting that the single crystal iridium with [100] orientation undergoes brittle fracture under a tensile loading at 1 K.

### 2.2.2 [110] orientation

The representative cutaway views of the [110] oriented single crystal iridium at various strains are displayed in Fig.4. The yielding occurs at a strain level of 0.095 (see Fig.2), displaying a relatively organized atomistic arrangement in Fig.4a due to few displacements of iridium atoms. When increasing the strain to 0.098, the stress declines sharply on stress-strain curve (see Fig.2). Configuration analysis from Fig.4b shows that stacking faults are formed. For further observing those stacking faults, the atoms were colored via Common Neighbor Analysis (CNA) method on OVITO. As presented in Fig.5, the atoms on fcc lattice are colored in green stacking by ABCABCABC..., meanwhile the atoms on hcp lattice are colored in red stacking by ABABAB..., while the atoms on other lattice structures are colored in white. Once atomic stacking order in the fcc lattice is wrong and becomes ABCABABCABC ..., red atoms on hcp lattice emerge. Hence, the first sharp drop in stress results from stacking faults during the tensile deformation of [110] single crystal iridium at 1 K. At strain of 0.171, namely, the strain corresponding to the second drop sharply declines in stress, and a relatively flat fracture can be observed in Fig.4c, which denotes that the [110] oriented single crystal iridium still exhibits brittle fracture mode under tension at 1 K.

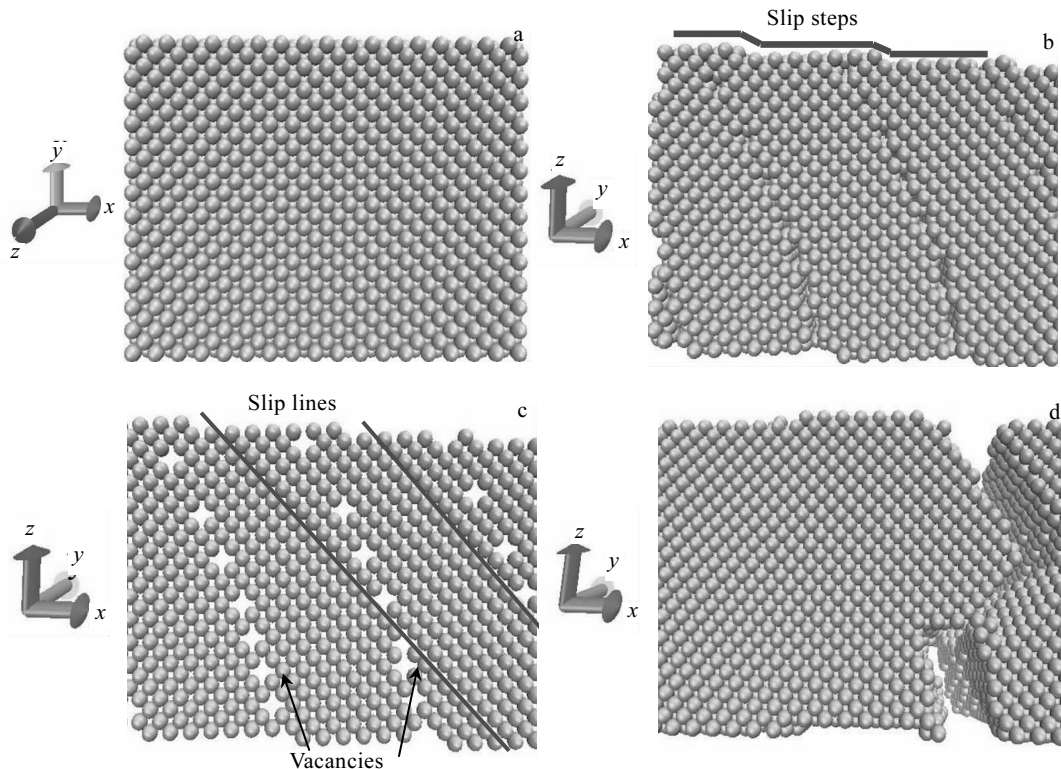


Fig.3 Cutaway views of [100] oriented single crystal iridium at strain levels of 0.093 (a), 0.095 (b, c), and 0.138 (d)

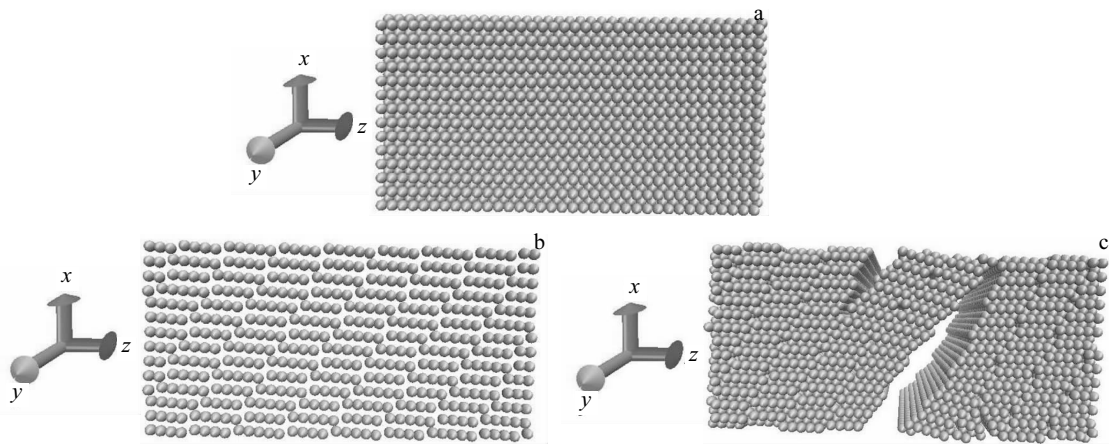


Fig.4 Cutaway views of [110] oriented single crystal iridium at strain levels of 0.095 (a), 0.098 (b), and 0.171 (c)

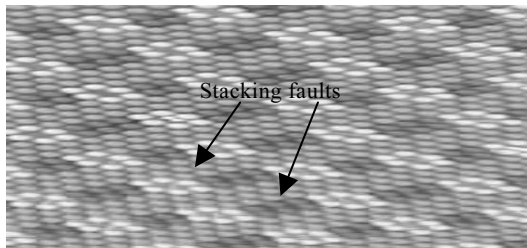


Fig.5 CNA diagram of [110] oriented single crystal iridium at a strain level of 0.098%

2.2.3 [111] orientation

The cutaway view of various strain levels during the tensile deformation of [111] single crystal iridium is shown in Fig.6. Fig.6a illustrates the atomic arrangement in the elastic deformation stage at a strain level of 0.02. It can be found that the atoms are arranged regularly and uniformly

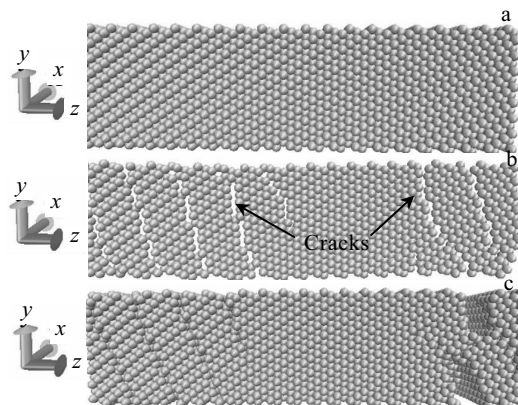


Fig.6 Cutaway views of [111] oriented single crystal iridium at strain levels of 0.02 (a), 0.121 (b), and 0.123 (c)

stretched along the z axis. When increasing the strain to 0.121, atomic configuration in Fig.6b depicts that some multiple cracks take place in single crystal iridium, which results in a dramatic decline in stress. At even higher strains, the model fractures eventually along [111] plane at the strain of 0.123 (see Fig.6c). There is little plastic deformation in [111] oriented single crystal iridium throughout the tensile deformation.

3 Conclusions

1) The tensile deformation behaviors of single crystal iridium are found to be orientation-dependent at 1 K. Mechanical properties (including elastic modulus, yield stress, ultimate tensile stress and elongation) obtained from stress-strain relationships are more or less different in [100], [110] and [111] crystallographic orientations.

2) Plastic deformation mechanism varies in crystallographic orientations. Under tensile loading, the single crystal iridium with [100] orientation mainly deforms by dislocation sliding as well as partial vacancy coalescence, while the plastic deformation in [110] single crystal iridium is mainly caused by stacking faults. However, there is little plastic deformation in [111] oriented single crystal iridium before breaking.

References

- 1 Hunt L B. *Platinum Metals Review*[J], 1987, 31(1): 32
- 2 Hecker S S, Rohr D L, Stein D F. *Metallurgical Transactions A*[J], 1978, 9(4): 481
- 3 Liu Y, Liu C T, Heatherly L et al. *Journal of Alloys and Compounds*[J], 2008, 459(1): 130
- 4 Wang Peng, Yu Jie, Zhou Xiaolong et al. *Rare Metal Materials and Engineering*[J], 2015, 44(10): 2363
- 5 Brookes C A, Greenwood J H, Routbort J L. *Journal of Applied Physics*[J], 1968 39(5): 2391

- 6 Hieber H, Mordike B L, Haasen P. *Platinum Metals Review*[J], 1964, 8(3): 102
- 7 Panfilov P, Yermakov A, Antonova O V et al. *Platinum Metals Review*[J], 2009, 53(3): 138
- 8 Panfilov P, Yermakov A. *Platinum Metals Review*[J], 2001, 45(4): 176
- 9 Yermakov A, Panfilov P, Adamesku R. *Journal of Materials Science Letters*[J], 1990, 9(6): 696
- 10 Panfilov P. *Journal of Materials Science*[J], 2007, 42(19): 8230
- 11 Sainath G, Choudhary B K. *Computational Materials Science*[J], 2016, 111: 406
- 12 Yuan Lin, Jing Peng, Shan Debin et al. *Philosophical Magazine*[J], 2016, 98(22): 2397
- 13 Ikeda H, Qi Y, Cagin T et al. *Physical Review Letters*[J], 1999, 82(14): 2900
- 14 Sturgeon J B, Laird B B. *Physical Review B*[J], 2000, 62(22): 14 720
- 15 Yang Zhenyu, Lu Zixing, Zhao Yapu. *Computational Materials Science*[J], 2009, 46(1): 142
- 16 Kondo Y, Takayanagi K. *Science*[J], 2000, 289(5479): 606
- 17 Liu Yunhong, Zhao Jianwei. *Computational Materials Science*[J], 2011, 50(4): 1418
- 18 Gao Yajun, Wang Hongbo, Zhao Jianwei et al. *Computational Materials Science*[J], 2011, 50(10): 3032
- 19 Liu Y H, Wang F Y, Zhao J W et al. *Physical Chemistry Chemical Physics*[J], 2009, 11(30): 6514
- 20 Sankaranarayanan S, Bhethanabotla V R, Joseph B. *Physical Review B*[J], 2007, 76(13): 134 117
- 21 Sun Yinlu, Sun Wei, Fu Yingqiang et al. *Computational Materials Science*[J], 2013, 79: 63
- 22 Zhang Y, Yu D J, Wang K M. *Journal of Materials Processing Technology*[J], 2012, 28(2): 164
- 23 Lin Yuanching, Pen Darjen. *Nanotechnology*[J], 2007, 18(39): 395 705
- 24 Ji Changjiang, Harold S P. *Nanotechnology*[J], 2007, 18(305704): 410
- 25 Park H S, Gall K, Zimmerman J A. *Journal of the Mechanics & Physics of Solids*[J], 2006, 54(9): 1862
- 26 Ferah G, Colakoglu K, Ciftci Y O et al. *Central European Journal of Physics*[J], 2007, 5(2): 207
- 27 Cawkwell M J, Nguyen-Manh D, Woodward C. *Acta Materialia*[J], 2007, 55(1): 161
- 28 Sheng H W, Kramer M J, Cadien A et al. *Physical Review B*[J], 2011, 83(13): 134 118
- 29 Allen M P, Tildesley D J. *Computer Simulation of Liquids*[M]. Oxford: Oxford University Press, 1987: 385
- 30 Plimpton S. *Journal of Computational Physics*[J], 1994, 117(2): 1
- 31 Reed T M, Gubbins K E. *Applied Statistical Mechanics: Thermodynamic and Transport Properties of Fluids*[M]. New York: McGraw-Hill Book Company, 1973: 25
- 32 Stukowski A. *Modeling and Simulation in Materials Science and Engineering*[J], 2010, 18: 15 012
- 33 Swope W C, Anderson H C, Berens P H et al. *Journal of Chemical Physics*[J], 1982, 76(1): 637

## 单晶铌取向有关的拉伸变形行为的原子尺度模拟

杨劫人<sup>1</sup>, 王虎<sup>1</sup>, 胡锐<sup>1</sup>, 张璠<sup>3</sup>, 李双明<sup>1</sup>, 刘毅<sup>2</sup>, 罗锡明<sup>2</sup>

(1. 西北工业大学 凝固技术国家重点实验室, 陕西 西安 710072)

(2. 昆明贵金属研究所, 云南 昆明 650106)

(3. 宝鸡文理学院, 陕西 宝鸡 721016)

**摘要:** 单晶铌与其它面心立方金属相比表现出反常的变形行为, 其本征变形断裂机制仍存在争议。本文进行分子动力学模拟研究了单晶铌在 1 K 下沿[100]、[110]和[111]取向的拉伸变形行为。研究表明: 单晶铌在 3 个取向应力-应变曲线上的变形行为差异明显。由于变形机制不同, 包括弹性模量、屈服强度、抗拉强度以及延伸率在內的力学性能在几个拉伸取向上或多或少存在差异。在拉伸载荷作用下, [100]取向单晶铌变形主要通过位错滑移还有少量空位聚集; [110]取向的塑性变形由堆垛层错引起; 而 [111]取向单晶铌断裂前产生的塑性变形量很少。

**关键词:** 单晶铌; 分子动力学; 拉伸变形; 晶体取向

作者简介: 杨劫人, 男, 1984 年生, 博士, 副教授, 西北工业大学凝固技术国家重点实验室, 陕西 西安 710072, 电话: 029-88492172, E-mail: yangjieren@nwpv.edu.cn